
Efficient Video Object Segmentation with Compressed Video

Kai Xu, Angela Yao
National University of Singapore
{kxu, ayao}@comp.nus.edu.sg

Abstract

We propose an efficient inference framework for semi-supervised video object segmentation by exploiting the temporal redundancy of the video. Our method performs inference on selected keyframes and makes predictions for other frames via propagation based on motion vectors and residuals from the compressed video bitstream. Specifically, we propose a new motion vector-based warping method for propagating segmentation masks from keyframes to other frames in a multi-reference manner. Additionally, we propose a residual-based refinement module that can correct and add detail to the block-wise propagated segmentation masks. Our approach is flexible and can be added on top of existing video object segmentation algorithms. With STM with top-k filtering as our base model, we achieved highly competitive results on DAVIS16 and YouTube-VOS with substantial speedups of up to 4.9X with little loss in accuracy.

1 Introduction

Video object segmentation (VOS) aims to obtain pixel-level masks of the objects in a video sequence. State-of-the-art methods [17, 18, 20, 22] using deep learning are highly accurate at segmenting the objects, but due to the deep networks used, can be slow, requiring as much as 0.2 seconds [20] to segment a frame. More efficient methods [25, 34, 3] then typically trade off accuracy for speed. We aim to develop an accurate yet efficient video object segmentation framework. Given the large frame-to-frame redundancies in a video sequence, we follow a propagation-based approach in which a (heavy) base network is applied to only keyframes. The resulting segmentations are then propagated to non-keyframes and refined with a lightweight network.

Propagation-based approaches are common in video semantic segmentation [13, 16, 21, 42] but are little explored for efficient VOS [15] due to several reasons. Firstly, the selection of keyframes is non-trivial. For maximum efficiency, keyframes should be as few and distinct as possible; yet if they are too distinct, the gap becomes too large to propagate across. As a result, existing works select keyframes conservatively with either uniform sampling [42, 13] or thresholding of changes in low-level features [16]. A second reason is that propagating segmentation masks relies on optical flow and computing accurate flow fields [11, 31] is still computationally expensive. Most importantly, propagated masks are usually insufficient in accuracy. Optical flow is often inaccurate around object borders and areas of occlusion and such errors compound over multiple frames. As a result, extensive refinement must be applied; in fact, in some methods [13], the refinement network is almost as heavy as the keyframes' base network, leaving little efficiency to be gained.

In this work, we propose to leverage compressed video for propagation-based VOS. Video compression encoders take a sequence of raw images as input and output a compressed form that exploits the inherent spatial and temporal redundancies in the sequence. The compressed bitstream offers “free” sources of information that largely resolve each of the previously discussed drawbacks. First, the image type (I- vs. P-/B-frames) gives some indication for keyframes, as the encoder separates the

frames according to their information content. Secondly, the motion compensation scheme used in compression directly provides motion vectors that can serve as a cheap approximation to optical flow. While motion vectors are coarser than optical flow, they are inherently bi-directional and reference both previous and future frames. As a result, masks propagated using motion vectors, while not as detailed as optical flow, suffer from less drift and occlusion errors. Finally, the residuals from the motion compensation give a strong indicator of difficult areas which may require refinement.

Putting all of this together, we design a new framework for efficient VOS using compressed video. We apply standard methods [20, 27, 4] as base networks to segment keyframes and then leverage the motion vectors to propagate the segmentations and residuals to help with refinement. A key difference between existing propagation methods [42, 21, 22, 19] and our method is that our propagation scheme is bi-directional. This allows us to efficiently generate masks which are, while coarse, more accurate. In turn, this enables a lightweight refinement guided by the residuals.

Our propagation and refinement scheme is highly flexible. It can be placed on top of almost any type of base VOS network and achieves up to 6X speed-up with minimal drops in segmentation accuracy. As a by-product of our keyframe selection, we are able to reduce the memory of memory-networks [20, 27], which are some of the fastest and most accurate state-of-the-art VOS methods. We summarize our contributions below:

- We propose a highly-efficient VOS framework that leverages information from the compressed video bitstream. At its core is a segmentation propagation scheme based on bi-directional motion vectors which yields highly accurate warps across multiple references.
- We propose a lightweight refinement module based on the motion compensation residuals to correct for propagation errors and artifacts.
- Our framework is flexible and can be inserted on top of standard VOS methods to achieve up to 4.9X speedup with negligible drops in accuracy. Experiments verify that we achieve highly competitive segmentation accuracies on DAVIS16 and DAVIS17 at 70FPS.

2 Related Work

Video object segmentation We limit our discussion to semi-supervised methods in which an initial mask is provided for the video sequence. Matching-based VOS methods rely on limited appearance changes, to either match the template and target frame, or to learn an object detector. For example, [1, 33, 25] fine-tune a segmentation network using the provided and estimated masks with extensive data augmentation. Other examples include memory networks [20, 27] that perform reference-query matching for the target object based on features extracted from previous frames.

Propagation methods rely on temporal correlations to propagate segmentation masks from the annotated frames. A simple strategy for propagation is to copy the previous mask [22], assuming limited change from frame-to-frame. Others works use motion-based cues from optical flow [32, 5, 10]. Frame-wise propagation has also been leveraged for efficient semantic video segmentation [42, 13, 21]. Our proposed framework is propagation-based, but we differ in that we leverage the compressed video bitstream for propagation and refinement. We adaptively select key-frames and our work is the first to use bi-directional motion vectors for mask warping.

Compressed videos in vision Compressed videos has been explored in computer vision for various tasks including object detection [35], object segmentation [30], saliency detection [39] and action recognition [38]. These works leverage information from the compressed video bitstream such as motion vectors and residuals as motion cues or bit allocation as indicators of saliency.

The work most similar to ours in spirit is [30], which also used motion vectors from compressed video for frame-wise propagation in video object segmentation. However, they choose a highly restrictive encoder setting that uses only I- and P-frames. This significantly simplifies their motion handling as it reduces the motion compensation to be uni-directional, with only a single reference point in the I-frame itself. As a result, the propagated masks of [30] are very low in accuracy. Additionally, the applicability of their framework is highly limited, as any modern video codec is B-frame dominated. In contrast, our framework leverages the valuable bi-directional motion information in B-frames and allows us to propagate highly accurate masks across multiple reference frames.

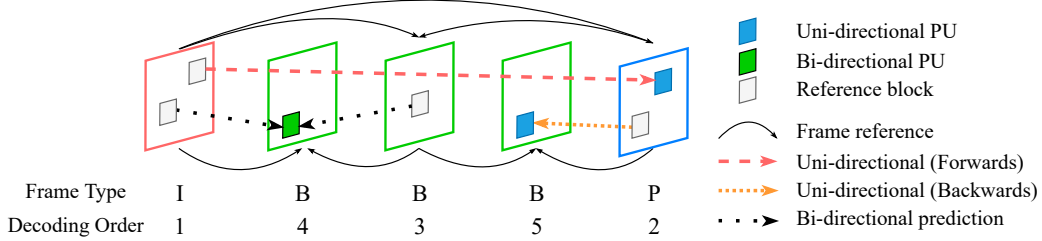


Figure 1: Compressed video sequence with dashed lines denoting motion compensation in PU blocks.

3 Preliminaries on Video Compression

3.1 Compressed Video Format

Video in raw form is a sequence of RGB images; however, it is unnecessary to store all the (image) frames. Video compression (en)coder-decoders, or codecs, leverage frame-to-frame redundancies to minimize storage. We outline some essentials of the HEVC codec [28] though other codecs such as MPEG [14] and H.264 [37] follow similar principles. Note that this section introduces only points relevant for understanding our framework; we refer to [29] for a more comprehensive treatment.

The HEVC coding structure consists of a series of frames called a Group of Pictures (GOP). Each GOP contains one or more I-frames, multiple P- and B-frames, and residuals for each P- and B-frame. I-frames are RGB images, while P- and B-frames encode information to recover their RGB content via motion compensation.

Specifically, the P- and B-frames store motion vectors, which can be considered a block-wise analogue of optical flow between that frame and its reference frame(s) in the GOP. Any discrepancies not compensated are then stored in that frame's residual. Video decoding is therefore done in an order to ensure that reference frames are decoded first to preserve the chain of dependencies. Fig. 1 illustrates the dependencies in a sample sequence.

3.2 Motion compensation in compressed video

A key difference between optical flow and motion vectors is that optical flow is a dense vector field, whereas motion vectors store block-wise displacements with respect to some reference frame(s). The associated blocks are referred to as a Prediction Unit (PU). PUs range in size from 64×64 to 8×4 or 4×8 pixels. PUs can be uni-directional, with reference frames from either the past or the future, or bi-directional, with two motion vectors referencing past and future frames. P-frames have only uni-directional PUs, while B-frames can have both uni-directional and bi-directional PUs.

More specifically, the unidirectional motion vector of a PU, $\mathbf{v} \in \mathbb{R}^3$, located at frame i with pixel indices $(x, y) \in \Omega$ is defined as a block-wise motion for all constituent pixels, *i.e.* $\mathbf{v}(\Omega, i) = [v_x, v_y, r]$. As such, pixels at (Ω, i) can be predicted using a co-located block of the same size in reference frame I_r at frame r , translated by $[v_x, v_y]$. Bi-directional PUs are associated with two motion vectors $(\mathbf{v}, \mathbf{v}')$ along with respective weighting components (ω, ω') used in the reconstruction, *i.e.*

$$\hat{I}_i(x, y, \mathbf{v}, \mathbf{v}') = \omega I_r(x + v_x, y + v_y) + \omega' I_{r'}(x + v'_x, y + v'_y), \quad (x, y) \in \Omega, \quad \omega + \omega' = 1, \quad (1)$$

where \hat{I}_i is the reconstructed image at frame i and \mathbf{v} and \mathbf{v}' indicate the motion vectors with past and future reference frames respectively. In the case of a uni-directional PU, either v or v' as well as ω or ω' would be 0. Examples of uni-directional and bi-directional PUs are illustrated in Fig. 1.

Motion-vectors are inherently coarse and noisy. As they encode only block-wise differences, image reconstructions tend to be inaccurate at PU boundaries and have block-like artifacts. Also, the encoder may fail in estimating accurate motions, especially for fast and abrupt movements (see examples in Fig. 2). Differences between the original RGB image and reconstruction at frame i are stored in the residual $\mathbf{e}_i = I_i - \hat{I}_i$, so pixel-level detailing can still be recovered. The key to efficient video encoding is balancing the storage savings of using larger PUs for P- and B-frames, *i.e.* fewer motion vectors, versus requiring denser residuals to compensate for the coarser block motions.

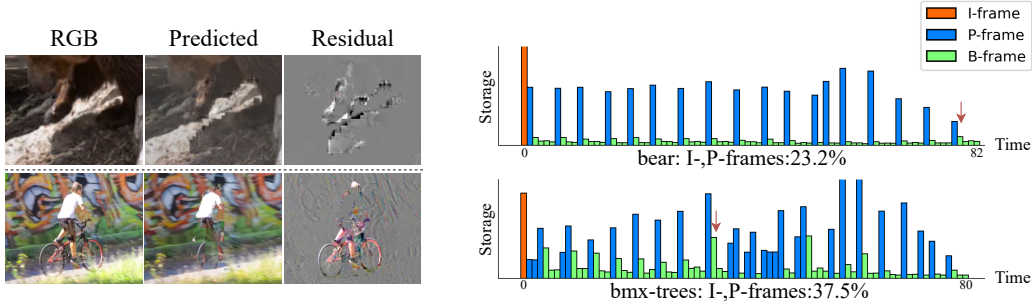


Figure 2: Left: Artifacts for ‘bear’ (top, has block effects) and ‘bmx-trees’ (bottom, motion vector estimation failure) sequence from DAVIS16. Right: Bar plots show frame assignments and storage of the frames over the two sequences, indicating dynamic content. ‘bmx-trees’ features fast movements and has more I-/P-frames than ‘bear’. The red arrows marks the corresponding frames on the left.

4 Methodology

We apply a base network (Sec. 4.1) to selected keyframes to extract segmentation masks; these masks are propagated to the non-key frames which are then further refined via a refinement network (Sec. 4.3). Masks are propagated (Sec. 4.2) to non-keyframes via warping, based on the motion vectors. Fig. 3 illustrates the overall structure for our framework.

4.1 Choice of keyframes & base network

We denote the reconstructed image sequence from a compressed video bit stream of length $T + 1$ as $\{(f_i, Z_i), i \in [0, T]\}$, where f_i denotes the reconstructed RGB image of frame i and Z_i is an indicator denoting the frame type *i.e.* as an I-, P- or B-frame. Parallel to the RGB reconstruction for each frame, raw motion vector fields and residuals $\{(M_i, E_i), i \in [0, T]\}$ are extracted for all non-I-frames. For a frame i which is a keyframe, we generate the foreground-background segmentation S_i from a base model, *i.e.* $S_i = N(f_i) \in \mathbb{R}^{(K+1) \times H \times W}$ where K is the number of objects in the video sequence and $H \times W$ is the segmentation mask resolution.

In principle, any frame can be used as a keyframe. However, as the encoder designates frame types based on the video’s dynamic content and designates as P- and especially B-frames the frames with higher redundancy. It is therefore natural to define keyframes according to the frame type and in our work, we choose both I- and P-frames as keyframes. In the default HEVC encoding, less than 5% of frames in a video sequence are I-frames; for accurate propagation, we require the additional 15-35% of frames designated as P-frames for keyframes. As the motion compensation in P-frames is strictly uni-directional, propagation from these frames may suffer inaccuracies arising from occlusions (in the same manner as optical flow). The occlusions in P-frames are encoded in forms¹ other than PUs; this results in holes in the motion vector field and would require additional handling.

The choice in base model N is flexible; all detection or matching-based models are suitable as they rely only on the appearance of the target object. From preliminary experiments, we observe that memory-based video segmentation methods such as STM [20] and KMN [27] work well as base models. Conveniently, the choice of using I-/P-frames as keyframes is well-suited for memory-networks because it naturally acts as a selection for having a compact yet diverse memory.

4.2 Mask propagation using motion-vector warping

To propagate segmentation masks to non-keyframes, we use the decoded motion vectors to warp existing segmentation masks onto B-frames. First, we define a generalized bi-directional motion field for a given frame i based on the associated bi-directional PU’s raw motion vectors:

$$[\mathbf{M}_i; \mathbf{M}'_i] = [V_{i,x}, V_{i,y}, R_i; V'_{i,x}, V'_{i,y}, R'_i], \quad (2)$$

where the first three terms compose the reconstructed motion field from various PUs in the forward direction for \mathbf{M}_i while the second three terms compose the reconstructed motion field in the backward

¹Intra-prediction blocks and skip blocks are currently not handled in our framework.

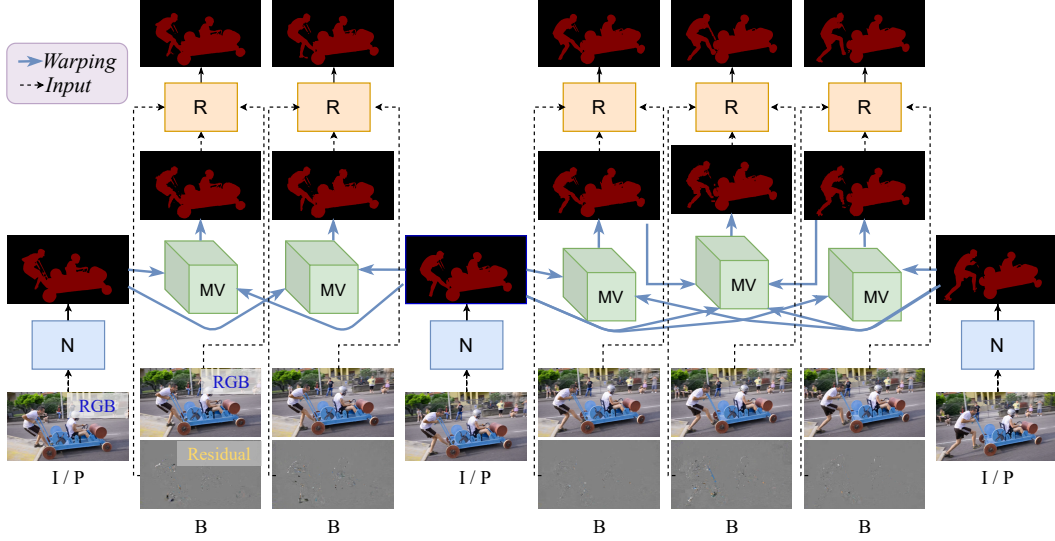


Figure 3: Overall framework. N : Base model. MV : Motion vector-based propagation. R : Refinement model. Segmentations of the I/P keyframes from the base model are propagated to the B non-keyframes. Propagated masks are further refined based on the RGB image and residuals.

direction M'_i . Note that all the elements of R_i are less than i , while all the elements of R'_i are greater than i . In the case that a given PU in the B-frame is uni-directional, then that element in the opposite direction in either M_i or M'_i is set to zero accordingly.

The reference mask elements to be propagated can be derived from either the base network applied to keyframes, or to propagated segmentation masks of previous reference frames. For notation simplicity, we refer to both types of masks simply as the S_r for some reference frame r . The warping however is a reverse-mapping procedure that must follow the decoding order Γ , *i.e.* warping mask elements based on already-decoded frames in the GOP with existing segmentation masks, which we refer to as the set S . For reverse-mapping, the propagated mask \hat{S}_i 's element at pixel location (m, n) for frame i can be defined as

$$\hat{S}_i(m, n) = \begin{cases} w(S, M_i, (m, n)), & \text{if } M'_i(m, n) = \mathbf{0}, \\ w(S, M'_i, (m, n)), & \text{if } M_i(m, n) = \mathbf{0}, \\ \frac{1}{2}w(S, M_i, (m, n)) + \frac{1}{2}w(S, M'_i, (m, n)), & \text{otherwise,} \end{cases} \quad (3)$$

where the warping function $w(\cdot)$ spatially interpolates the source frame's mask with function g :

$$w(S, M, (m, n)) = \sum_{\mathbf{q}} G(\mathbf{q}, (x + V_x(m, n), y + V_y(m, n))) \cdot S_{R_i(m, n)}(\mathbf{q}), \quad (4)$$

G can be any interpolation function kernel such as nearest-neighbours or bilinear interpolation and \mathbf{q} enumerates all spatial locations in the reference map. The first two cases in Eq. 3 can be used for warping unidirectional motion vectors forward and backward in time respectively while the third case is for bidirectional motion vectors. Note that in the third case, the forward and backward motion vector are equally weighted and not according to ω and ω' as defined in Eq.1. This is because we interpret the references to be equally indicative of the target mask; also ω and ω' are tuned for reconstructing the target RGB pixel value.

4.3 Residual-based refinement network

Motion vectors are coarse, and as shown in Fig. 2, can also be wrong. To improve the propagated masks, we introduce an additional refinement network. The use of additional refinement is common in propagation-based segmentation frameworks[22, 30]. As the errors of the motion vectors are captured inherently in each frame's residuals, it is natural to use these as a cue for refinement. We

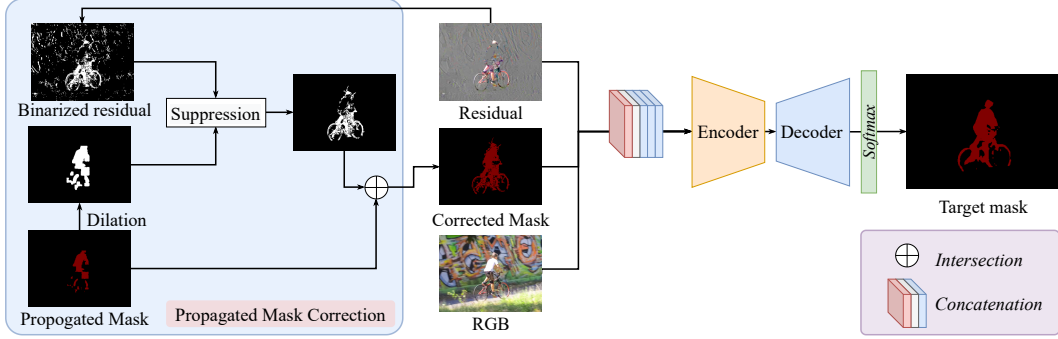


Figure 4: Refinement scheme composed of propagated mask correction and encoder-decoder network.

use a simple encoder-decoder plus soft-max layer. As input, we provide a concatenated stack of the recovered RGB frame, residual frame and the propagated mask. However, rather than giving the propagated mask directly, we perform a correction step based on the residual frame (see Fig. 4).

Propagated Mask Correction: Let \hat{S} and $e \in \mathbb{R}^{3 \times H \times W}$ denote the propagated mask and residuals at some given frame. We first convert e into a greyscale image before converting it into a binary mask e_b via thresholding. The corrected mask \tilde{S} is defined as $\tilde{S} = U(e_b, \hat{S}_+) \oplus \hat{S}$, where \hat{S}_+ indicates a dilated version of initially propagated mask and \oplus indicates a pixel-wise union operation. $U(a, b)$ indicates a suppression operation in which we retain only the connected components of a that overlap with b , *i.e.*, we keep only the components of the binarized residual which intersect with the dilated mask \hat{S}_+ . This allows us to recover detailing from the residual only in areas surrounding the object of interest indicated by the dilated mask. The mask correction helps only for cases of under-segmentation when the motion vectors are wrong and miss parts of the object of interest. In areas of over- and under-segmentation due to the block-wise nature of the motion vectors, we rely on the encoder-decoder for further refinement, presumably based on cues from the original RGB image.

4.4 Implementation Details

Video Compression We generate compressed video from images using the x265 library in FFmpeg on the *default* preset. To write out the bitstream information, we modify the decoder from openHEVC[9, 8] and share the code publicly² to encourage others to work with compressed video.

Base Model We advocate using STM [20] with top- k filtering [4] as the base model for our framework. STM stores features from previous segmentations in the memory and applies them to segment the current frame via an attention-based query operation. The top- k filtering reduces memory read out during inference to only k entries. For our work, we feed only the keyframes into the memory bank. In practice, this is equivalent to segmenting a temporally reduced video and reduces the memory. We experiment with other base-models [25] to verify the flexibility of our method.

Propagation & Refinement We use reverse mapping in our warping for propagation and experiment with bilinear and nearest interpolation kernels. For the encoder-decoder in the refinement, we use DeepLabv3plus[2] pretrained on Pascal VOC 2012[7] with MobileNetV2[26] as the backbone. The refinement network is trained on a mixture of DAVIS and YouTube-VOS data with learning rate $2e-4$ with a decay factor of 0.1 every 20k iterations for a total of 80k iterations.

5 Experimentation

5.1 Datasets & Evaluation

We report results on three video object segmentation benchmarks: DAVIS16[23] and DAVIS17[24] are small datasets, featuring 50 and 120 videos of single and multiple objects respectively, while YouTube-VOS[40] is large-scale, with 3945 videos of multiple objects. Videos from DAVIS are decoded from 1080p while segmentation is performed at 480p so we use the bilinear kernel for

²URL to be released.

Table 1: Comparison with state-of-the-art methods on DAVIS16, DAVIS17 and YouTube-VOS validation set. Note that previous works only report their FPS on DAVIS16; for DAVIS17 and YouTube-VOS, FPS is usually lower depending on how multiple objects are handled.

Method	DAVIS16 validation				DAVIS17 validation			
	\mathcal{J}	\mathcal{F}	$\mathcal{J}\&\mathcal{F}$	FPS	\mathcal{J}	\mathcal{F}	$\mathcal{J}\&\mathcal{F}$	FPS
OSVOS [1]	79.8	80.6	80.2	0.22	56.7	63.9	60.3	-
STM [20]	88.7	89.9	89.3	6.3	79.2	84.3	81.8	-
RGMP [19]	81.5	82.0	81.8	7.7	64.8	68.6	66.7	-
FRTM-VOS [25]	-	-	83.5	22	-	-	76.7	-
RANet [36]	85.5	85.4	85.5	30	63.2	68.2	65.7	-
SSM-VOS [41]	86.2	85.6	85.9	37	75.3	79.9	77.6	-
SAT [3]	82.6	83.6	83.1	39	68.6	76.0	72.3	-
FRTM-VOS-fast [25]	-	-	78.5	41	-	-	70.2	-
STM top- k [4] (Base Model)	89.7	92.4	91.0	17	81.7	87.4	84.5	11
CoVOS MV-Warp (Ours)	87.7	89.5	88.6	40	79.0	84.4	81.7	25
CoVOS MV-Warp + Refine (Ours)	89.3	91.3	90.3	29	79.5	84.8	82.2	21

Method	YouTube-VOS validation set					
	Overall	\mathcal{J}_{seen}	\mathcal{J}_{unseen}	\mathcal{F}_{seen}	\mathcal{F}_{unseen}	FPS
STM [20]	79.4	79.7	84.2	72.8	80.9	-
RGMP [19]	53.8	59.5	45.2	-	-	-
SSM-OVS [41]	66.5	72.3	73.3	57.8	62.6	-
SAT [25]	63.6	67.1	55.3	70.2	61.7	-
FRTM-VOS-fast [25]	65.7	68.6	58.4	71.3	64.5	-
KMN[27] top- k (Base Model)	82.8	81.6	77.7	85.8	85.9	8.3
CoVOS MV-Warp (Ours)	80.5	79.5	73.5	85.2	83.8	41
CoVOS MV-Warp + Refine (Ours)	81.2	80.7	74.9	85.6	83.5	28

propagation. Videos from YouTube-VOS are mostly 720p and decoded and segmented at the same original size so we use the faster nearest neighbour kernel for propagation. When multiple objects are present, we aggregate all labels into one plane, thus requiring only one pass for the refinement. The default HEVC encoding produces an average of {37%, 36%, 27%} of I/P-frames and therefore keyframes per sequence for DAVIS16, DAVIS17 and YouTube-VOS respectively.

We evaluate with the standard criteria from [23], using Jaccard Index \mathcal{J} (IoU of the output segmentation with ground-truth mask) for region similarity and mean boundary \mathcal{F} -scores for contour accuracy. Additionally, we report the average score over all seen and unseen classes for YouTube-VOS.

5.2 Comparison to State-of-the-Art

We compare with state-of-the-art models in Tables 1 and observe that our method achieves an excellent compromise between accuracy and speed. On DAVIS16 without refinement, we can run at 40FPS. Our performance is +2.7 to +10.1% higher than other efficient methods SSM-VOS [41], SAT [3] and the fast version of FRTM-VOS [25] which have comparable framerates, though much of this success should be attributed to the high accuracies of our base model STM top- k [4]. Without refinement, we achieve speedups of 2.3-2.4X from the base model with only a drop of 2.4 and 2.8 in $\mathcal{J}\&\mathcal{F}$ for DAVIS16 and 17 respectively. Adding refinement reduces the speedup to 1.7-1.9X but closes the gap to the base model to only 0.7 and 2.3. On YouTube-VOS, we use state-of-the-art KMN [27] top- k as the base model. Our method without refinement achieves a 4.9X speedup with only a 2.3% overall drop; with refinement the gap closes to 1.6% with a 3.4X speedup.

5.3 Ablation Studies

We first verify each component of our framework. All ablations use STM top- k as the base model on default video encode preset unless otherwise indicated; comparison between propagation methods and refinement steps are evaluated only on non-keyframes.

Propagation We compare with forwards optical flow warping, as done in [6, 22, 42], computing the flow with state-of-the-art RAFT [31]. We also compare with two motion vector baselines from [38] and [30]. The former in [38] converts motion vectors into a flow, *i.e.* for motion vector \mathbf{v} at (x, y) and frame i , $M_{of}(x, y) = [v_x, v_y]/[(r - i) \cdot fps]$ is the motion of the pixel (x, y) in the unit time on plane i . The latter [30] is further simplified and references all motions from one I-frame in the GOP.

Table 2 verifies the effectiveness of our proposed propagation. The warping of [38], designed originally to estimate motion features for action recognition, performs on par with optical flow. The simplified case of [30] fails to propagate meaningful segmentation masks. In contrast, our propagation is highly accurate and our warped masks are within 4.5 points on both \mathcal{J} and \mathcal{F} below the baseline without propagation, *i.e.* by applying each frame through the base network. From Fig. 5 we observe qualitatively that optical flow propagation and motion-vector generated flow both suffer from ghosting effects and holes in areas of occlusion. Our propagation, by leveraging multi-directional motion vectors and multiple reference frames within the GOP, successfully prevents such artifacts.

Refinement: Table 3 shows how adding each component of our refinement module leads to progressive improvements for the boundary \mathcal{F} -score, whereas the largest gains for the \mathcal{J} -index come from using the encoder-decoder. When we remove propagated mask correction, performance decreases, especially for the boundary \mathcal{F} -score. As the propagated results are already quite strong, the gains from the refinement are not significant; in settings where propagated results are lower, *e.g.* when there are fewer keyframes, the impact of the refinement is much stronger (see Table 4). Fig.5 shows qualitative results of different propagation methods as well as our refinement network.

Table 2: Comparison of Propagation Methods

Method	DAVIS16		DAVIS17	
	\mathcal{J}	\mathcal{F}	\mathcal{J}	\mathcal{F}
Optical Flow	70.0	73.9	66.4	73.0
I to P-frame[30]	31.5	-	-	-
MV to Flow [38]	70.2	72.2	63.4	71.2
MV Warp (ours)	86.4	88.6	78.1	83.9
No propagation [4]	90.1	92.9	82.1	88.0

Table 3: Refinement ablations on DAVIS16

Module	\mathcal{J}	\mathcal{F}
MV Warp	86.4	88.6
+ Mask Correction	86.7	89.1
+ Refine (RGB)	88.8	90.3
+ Refine (RGB+Residual)	88.9	91.0
+ YouTube-VOS	88.9	91.5
Refine w/o Correction	88.7	90.9

Table 4: Robustness to different video encoding preset on DAVIS16, B-frame biased: more weight on B-frame allocation, uniform b-frames: fix 8 b-frames between I/P frames.

Encoder Preset	Keyframe	MV Warp			Res Refine		
		\mathcal{J}	\mathcal{F}	FPS	\mathcal{J}	\mathcal{F}	FPS
Default	37.3%	87.7	89.5	40	89.3	91.3	29
B-frame biased	19.3%	83.7	85.8	72	87.3	89.3	40
Uniform B-frames	13.2%	78.0	79.7	100	84.2	85.4	43

Keyframe percentage To highlight speed-accuracy trade-off, we compare the percentage of keyframes in Table 4 by adjusting encoder presets. The default HEVC setting yields 37.3% keyframes for DAVIS16. If we set the encoder to allocate more B-frames to have only 19.3% and 13.2% keyframes (*'B-frame biased'* and *'Uniform B-frames'* respectively), the propagated scores decreases while the FPS increases accordingly. Interestingly, our refinement can compensate for some of the drop so improvements from refinement also get progressively larger. At the fastest setting, we can achieve 100FPS video object segmentation with \mathcal{J} and \mathcal{F} scores of 78.0 and 79.7.

Additional base models. In Table 5, we apply our framework to other base models. With different presets, we speed up the original STM 6.3X to 40 FPS with competitive accuracies. For the FRTM [25] model, our speed-up is less impressive as FRTM performs online fine-tuning, which has significant overhead that cannot be reduced with fewer keyframes. Nevertheless, we achieve a speedup of 1.6X with refinement with negligible drops in accuracy.

Table 5: Speedup (S) on different base models with default and B-biased presets on DAVIS16. \dagger We are unable to reproduce the reported 22FPS of FRTM and report here our measured speed.

Base	Per-frame		Preset	MV Warp			Res Refine		
	$\mathcal{J} \mathcal{F}$	FPS		$\mathcal{J} \mathcal{F}$	FPS	S	$\mathcal{J} \mathcal{F}$	FPS	S
STM [20]	88.7 89.9	6.3	Default	85.5 86.2	19	3.1X	87.3 88.5	17	2.7X
			B-biased	81.2 82.2	40	6.3X	85.1 86.4	26	4.1X
FRTM [25]	83.7 83.4	17 \dagger	Default	80.2 80.9	36	2.1X	82.6 83.8	27	1.6X
			B-biased	76.4 77.5	40	2.3X	80.8 82.2	27	1.6X

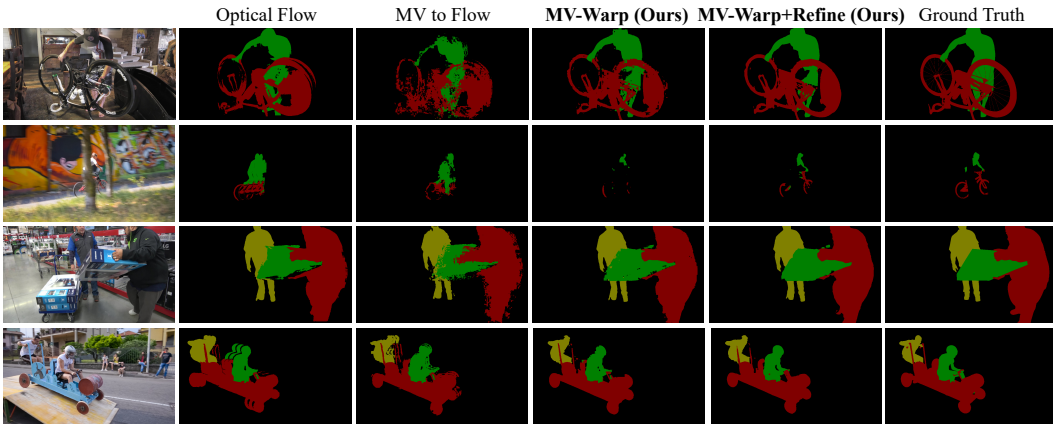


Figure 5: Qualitative results on different propagation methods and refinement.

5.4 Timing Analysis

To compute the FPS values in all our tables, we measure run times on an RTX-2080Ti. For sequences from DAVIS16 using STM top- k , we measure inference times of $54(\pm 9)$ ms for the base segmentation model (T_{base}), $5(\pm 2)$ ms for feature decoding (T_{decoding}), $0.1(\pm 0.01)$ ms for motion-vector warping (T_{warp}) and $14(\pm 1)$ ms for refinement (T_{refine}). We estimate an amortized per frame inference time based on $T_{\text{base}} \cdot R + (T_{\text{decoding}} + T_{\text{warp}} + T_{\text{refine}}) \cdot (1 - R)$ where R denote the ratio of keyframes. Note that our measured T_{base} may not correspond to published FPS values of base models that require online fine-tuning [25]. Additionally, for memory-network models like STM[20] and KMN[27], our T_{base} is lower as we store fewer frames in memory. For example, on YouTube-VOS, the memory is only one-third of the original based on its keyframe ratio. We refer to the Supplementary for further details.

6 Conclusion & Broader Impacts

We propose an efficient inference framework for semi-supervised VOS via propagation and refinement by exploiting the motion vectors and residuals of the compressed video bitstream. Such a framework can speed up accurate but slow base VOS models with minor drops in segmentation accuracy. One limitation of our work is the possible latency introduced by the multiple reference dependencies. As a result, segmentation results of a non-keyframe gets completed later than the future frame to which it refers, making our method ill-suited for online methods. As future work, we will investigate further improvements in efficiency by exploiting the spatial sparsity based on the compressed video’s frame-wise bit allocation.

Broader Impact: On a positive note, given that 70% of the internet traffic [12] is dedicated to (compressed) video, we see broad applicability of our work in making video methods more efficient. This is further compounded by the increasing spatial resolution of video, *e.g.* to 4K standards, especially for application scenarios of VOS such as video editing, making efficient handling is crucial. On the other hand, VOS may also be abused to falsify parts of videos or create malicious content. We maintain a rigorous attitude towards this while emphasizing its positive impact on content creation, and other possible improvements for society.

References

- [1] S. Caelles, K.-K. Maninis, J. Pont-Tuset, L. Leal-Taixé, D. Cremers, and L. Van Gool. One-shot video object segmentation. In *Proceedings of the IEEE conference on computer vision and pattern recognition*, pages 221–230, 2017.
- [2] L.-C. Chen, Y. Zhu, G. Papandreou, F. Schroff, and H. Adam. Encoder-decoder with atrous separable convolution for semantic image segmentation. In *Proceedings of the European conference on computer vision (ECCV)*, pages 801–818, 2018.
- [3] X. Chen, Z. Li, Y. Yuan, G. Yu, J. Shen, and D. Qi. State-aware tracker for real-time video object segmentation. In *Proceedings of the IEEE/CVF Conference on Computer Vision and Pattern Recognition*, pages 9384–9393, 2020.
- [4] H. K. Cheng, Y.-W. Tai, and C.-K. Tang. Modular interactive video object segmentation: Interaction-to-mask, propagation and difference-aware fusion. In *CVPR*, 2021.
- [5] J. Cheng, Y.-H. Tsai, S. Wang, and M.-H. Yang. Segflow: Joint learning for video object segmentation and optical flow. In *Proceedings of the IEEE international conference on computer vision*, pages 686–695, 2017.
- [6] A. Dosovitskiy, P. Fischer, E. Ilg, P. Hausser, C. Hazirbas, V. Golkov, P. Van Der Smagt, D. Cremers, and T. Brox. FlowNet: Learning optical flow with convolutional networks. In *Proceedings of the IEEE international conference on computer vision*, pages 2758–2766, 2015.
- [7] M. Everingham, L. Van Gool, C. K. Williams, J. Winn, and A. Zisserman. The pascal visual object classes (voc) challenge. *International journal of computer vision*, 88(2):303–338, 2010.
- [8] W. Hamidouche, M. Raulet, and O. Déforges. Parallel shvc decoder: Implementation and analysis. In *2014 IEEE International Conference on Multimedia and Expo (ICME)*, pages 1–6. IEEE, 2014.
- [9] W. Hamidouche, M. Raulet, and O. Déforges. Real time shvc decoder: Implementation and complexity analysis. In *2014 IEEE International Conference on Image Processing (ICIP)*, pages 2125–2129, 2014.
- [10] P. Hu, G. Wang, X. Kong, J. Kuen, and Y.-P. Tan. Motion-guided cascaded refinement network for video object segmentation. In *Proceedings of the IEEE Conference on Computer Vision and Pattern Recognition*, pages 1400–1409, 2018.
- [11] E. Ilg, N. Mayer, T. Saikia, M. Keuper, A. Dosovitskiy, and T. Brox. FlowNet 2.0: Evolution of optical flow estimation with deep networks. In *Proceedings of the IEEE conference on computer vision and pattern recognition*, pages 2462–2470, 2017.
- [12] C. V. N. Index. Forecast and methodology, 2016–2021. *White paper, Cisco public*, 6, 2017.
- [13] S. Jain, X. Wang, and J. Gonzalez. Accel: A corrective fusion network for efficient semantic segmentation on video. In *CVPR*, 2019.
- [14] D. Le Gall. Mpeg: A video compression standard for multimedia applications. *Communications of the ACM*, 34(4):46–58, 1991.
- [15] Y. J. Lee, J. Kim, and K. Grauman. Key-segments for video object segmentation. In *2011 International conference on computer vision*, pages 1995–2002. IEEE, 2011.
- [16] Y. Li, J. Shi, and D. Lin. Low-latency video semantic segmentation. In *Proceedings of the IEEE Conference on Computer Vision and Pattern Recognition*, pages 5997–6005, 2018.
- [17] J. Luiten, P. Voigtlaender, and B. Leibe. Premvos: Proposal-generation, refinement and merging for video object segmentation. In *Asian Conference on Computer Vision*, pages 565–580. Springer, 2018.
- [18] K.-K. Maninis, S. Caelles, Y. Chen, J. Pont-Tuset, L. Leal-Taixé, D. Cremers, and L. Van Gool. Video object segmentation without temporal information. *IEEE Transactions on Pattern Analysis and Machine Intelligence*, PP, 09 2017.
- [19] S. W. Oh, J.-Y. Lee, K. Sunkavalli, and S. J. Kim. Fast video object segmentation by reference-guided mask propagation. In *Proceedings of the IEEE conference on computer vision and pattern recognition*, pages 7376–7385, 2018.

- [20] S. W. Oh, J.-Y. Lee, N. Xu, and S. J. Kim. Video object segmentation using space-time memory networks. In *Proceedings of the IEEE/CVF International Conference on Computer Vision*, pages 9226–9235, 2019.
- [21] M. Paul, C. Mayer, L. V. Gool, and R. Timofte. Efficient video semantic segmentation with labels propagation and refinement. In *Proceedings of the IEEE/CVF Winter Conference on Applications of Computer Vision*, pages 2873–2882, 2020.
- [22] F. Perazzi, A. Khoreva, R. Benenson, B. Schiele, and A. Sorkine-Hornung. Learning video object segmentation from static images. In *Proceedings of the IEEE conference on computer vision and pattern recognition*, pages 2663–2672, 2017.
- [23] F. Perazzi, J. Pont-Tuset, B. McWilliams, L. Van Gool, M. Gross, and A. Sorkine-Hornung. A benchmark dataset and evaluation methodology for video object segmentation. In *Computer Vision and Pattern Recognition*, 2016.
- [24] J. Pont-Tuset, F. Perazzi, S. Caelles, P. Arbeláez, A. Sorkine-Hornung, and L. Van Gool. The 2017 davis challenge on video object segmentation. *arXiv:1704.00675*, 2017.
- [25] A. Robinson, F. J. Lawin, M. Danelljan, F. S. Khan, and M. Felsberg. Learning fast and robust target models for video object segmentation. In *Proceedings of the IEEE/CVF Conference on Computer Vision and Pattern Recognition (CVPR)*, 2020.
- [26] M. Sandler, A. Howard, M. Zhu, A. Zhmoginov, and L.-C. Chen. Mobilenetv2: Inverted residuals and linear bottlenecks. In *Proceedings of the IEEE conference on computer vision and pattern recognition*, pages 4510–4520, 2018.
- [27] H. Seong, J. Hyun, and E. Kim. Kernelized memory network for video object segmentation. In *European Conference on Computer Vision*, pages 629–645. Springer, 2020.
- [28] G. J. Sullivan, J.-R. Ohm, W.-J. Han, and T. Wiegand. Overview of the high efficiency video coding (hevc) standard. *IEEE Transactions on Circuits and Systems for Video Technology*, 22(12):1649–1668, 2012.
- [29] V. Sze, M. Budagavi, and G. J. Sullivan. High efficiency video coding (hevc). In *Integrated circuit and systems, algorithms and architectures*, volume 39, page 40. Springer, 2014.
- [30] Z. Tan, B. Liu, W. Li, and N. Yu. Real time compressed video object segmentation. In *2019 IEEE International Conference on Multimedia and Expo (ICME)*, pages 628–633. IEEE, 2019.
- [31] Z. Teed and J. Deng. Raft: Recurrent all-pairs field transforms for optical flow. In *European Conference on Computer Vision*, pages 402–419. Springer, 2020.
- [32] D. Tsai, M. Flagg, A. Nakazawa, and J. M. Rehg. Motion coherent tracking using multi-label mrf optimization. *International journal of computer vision*, 100(2):190–202, 2012.
- [33] P. Voigtlaender and B. Leibe. Online adaptation of convolutional neural networks for video object segmentation. *arXiv preprint arXiv:1706.09364*, 2017.
- [34] Q. Wang, L. Zhang, L. Bertinetto, W. Hu, and P. H. Torr. Fast online object tracking and segmentation: A unifying approach. *arXiv preprint arXiv:1812.05050*, 2018.
- [35] S. Wang, H. Lu, and Z. Deng. Fast object detection in compressed video. In *Proceedings of the IEEE/CVF International Conference on Computer Vision*, pages 7104–7113, 2019.
- [36] Z. Wang, J. Xu, L. Liu, F. Zhu, and L. Shao. Ranet: Ranking attention network for fast video object segmentation. In *2019 IEEE/CVF International Conference on Computer Vision (ICCV)*, pages 3977–3986, 2019.
- [37] T. Wiegand, G. J. Sullivan, G. Bjontegaard, and A. Luthra. Overview of the h. 264/avc video coding standard. *IEEE Transactions on circuits and systems for video technology*, 13(7):560–576, 2003.
- [38] C.-Y. Wu, M. Zaheer, H. Hu, R. Manmatha, A. J. Smola, and P. Krähenbühl. Compressed video action recognition. In *Proceedings of the IEEE Conference on Computer Vision and Pattern Recognition*, pages 6026–6035, 2018.
- [39] M. Xu, L. Jiang, X. Sun, Z. Ye, and Z. Wang. Learning to detect video saliency with hevc features. *IEEE Transactions on Image Processing*, 26(1):369–385, 2017.
- [40] N. Xu, L. Yang, Y. Fan, D. Yue, Y. Liang, J. Yang, and T. Huang. Youtube-vos: A large-scale video object segmentation benchmark. *arXiv preprint arXiv:1809.03327*, 2018.

- [41] W. Zhu, J. Li, J. Lu, and J. Zhou. Separable structure modeling for semi-supervised video object segmentation. *IEEE Transactions on Circuits and Systems for Video Technology*, 2021.
- [42] X. Zhu, Y. Xiong, J. Dai, L. Yuan, and Y. Wei. Deep feature flow for video recognition. In *Proceedings of the IEEE conference on computer vision and pattern recognition*, pages 2349–2358, 2017.